metals

MDPI

Article

Observation and Analysis of Metallic Interface Bridging and Self-Healing Under Electromagnetic Shocking Treatment

Qian Sun [1,2,3,*], Yaxuan Duan [1,2,3], Fanglei Wang [1,2,3], Weibing Jie [1,2,3] and Suohui Liang [1,2,3]

[1] Hubei Key Laboratory of Advanced Technology for Automobile Components, Wuhan University of Technology, Wuhan 430070, China; duanyx@whut.edu.cn (Y.D.); 333888@whut.edu.cn (F.W.); 362354@whut.edu.cn (W.J.); 347782@whut.edu.cn (S.L.)
[2] Hubei Collaborative Innovation Center for Automotive Components Technology, Wuhan University of Technology, Wuhan 430070, China
[3] Hubei Research Center for New Energy & Intelligent Connected Vehicle, Wuhan University of Technology, Wuhan 430070, China
* Correspondence: sq191113_2227@whut.edu.cn; Tel.: +86-17362312530

Abstract: While self-healing of metals and alloys facilitated by electromagnetic pulse (EMP) energy introduced by electropulsing has been widely reported, the in-depth mechanism is still ambiguous. Here, an approximate in-situ observation was designed to explore the effect of EMP energy induced by electropulsing on the alloy interface self-healing. Electromagnetic shocking treatment (EST) utilizing EMP energy was demonstrated to promote metallic interface bridging and self-healing. At local regions, flat surfaces turn into wavy ones, especially, while local interface bridging and self-healing are commonly observed, indicating a nonlinear surface pre-melting. Based on the assumed mass–spring–damping system of the pre-melted interfaces, the mechanisms of local interface bridging and self-healing under the EST are explored. This work provides new understanding about the interface self-healing mechanism by electropulsing, as well as new insights about the effect of pulse energy (such as EMP) on metallic interface complexion.

Keywords: interface bridging; interface self-healing; metals and alloys; surface pre-melting; electromagnetic shocking treatment

check for updates

Academic Editor: Sónia Simões

Received: 13 February 2025
Revised: 29 March 2025
Accepted: 5 April 2025
Published: 9 April 2025

Citation: Sun, Q.; Duan, Y.; Wang, F.; Jie, W.; Liang, S. Observation and Analysis of Metallic Interface Bridging and Self-Healing Under Electromagnetic Shocking Treatment. *Metals* **2025**, *15*, 422. https://doi.org/10.3390/met15040422

Copyright: © 2025 by the authors. Licensee MDPI, Basel, Switzerland. This article is an open access article distributed under the terms and conditions of the Creative Commons Attribution (CC BY) license (https://creativecommons.org/licenses/by/4.0/).

1. Introduction

Healing or self-healing of metals and alloys has the potential to affect many structural applications [1], especially for fatigue failure under cyclic loads [2]. To facilitate the in-situ self-healing, processes leading to a "local temporary directional mobility" should be a pre-requisite. However, in-situ self-healing of cracks and crack-initiating defects in the metals and alloys is usually difficult considering that solute atoms acting as healing agents are relatively small and generally have a relatively low mobility at the operating temperatures. At present, the most promising approaches to self-healing metals include autonomous healing [2,3] and assisted healing methods such as heating [4] and plastic deformation [5,6], as well as electric field with or without healing agent [7–12]. For example, Barr et al. [2] reported that fatigue cracks in the pure metals can undergo intrinsic self-healing at the nanoscale by the cold welding of the crack flank, which was induced by a combination of inhomogeneous local stresses and progressive migration of grain boundaries in the vicinity of the crack tip. Also, Lu et al. [3] proved that, under relatively low applied pressures, single-crystalline gold nanowires of diameters between 3 and 10 nm can be cold-welded together within seconds by mechanical contact alone. Without a high enough temperature

and applied pressure, the self-healing scale of the metals and alloys involved in the above studies is only at the nanoscale. Once the self-healing scale of the metals and alloys reaches the micron or millimeter scale, or even the macro scale, sufficient temperature or pressure seems necessary. For example, as to the cracking issue in laser powder bed fusion additive manufacturing, Hu et al. [4] reported a liquid-induced healing (LIH) post-process that enables complete healing of those micro cracks by inducing the solid–liquid phase transition at the cracking regions; they also revealed the mechanisms of remelted liquid fraction and isostatic pressure during crack healing processing in In738LC alloy prepared by laser powder bed fusion. Similarly, as to the interface bonding problem in the metal additive forging process, Sun et al. [5,6] systematically investigated the effect of plastic deformation or hot compression bonding on the interfacial microstructure evolution. They concluded that, for 14YWT alloys [13], recrystallization at the interface region characterized by strain-induced grain boundary bulging and subsequent bridging sub-boundary rotation is the dominant nucleation mechanism, and the nuclei will grow with the ongoing deformation, which contributes to the healing of the original bonding interface. Furthermore, Hosoi et al. [11] demonstrated that a high-density electric current field can be utilized to heal a fatigue crack at micron scale in stainless steel, and the crack closure and the bridging between the surfaces of the crack were caused around the vicinity of the crack tip. However, they did not make in-depth discussion about the crack healing and bridging mechanisms under the effect of a high-density electric current field. Then, considerable investigations were carried out to investigate the influence mechanism of an electric current field on the crack healing of metals and alloys, and concluded that electropulsing can repair the crack/void [11,14,15] by coupling the thermal effect and athermal effect. That is, the current crowding effect, which would promote local high temperature and also form compressive stress because of temperature gradient, mainly contributes to the healing of the crack/void.

Actually, electromagnetic pulse (EMP) energy introduced by magnetic pulse (pulsed magnetic field) [16–20], electric pulse (or electropulsing) [21–25] or laser pulse [26], has been widely utilized to modify the microstructure, properties and performance of metals and alloys. As is widely known, electropulsing can promote fast phase transition [27–31] and then affect the properties and performance of the metals and alloys. Most of the studies supported the finding that the local transient high temperature generated by electropulsing mainly results in the fast phase transition [28,29,31], while the effect of the athermal effects of electropulsing on the microstructure evolution of the metals and alloys has also gained the attention of some researchers [32,33]. For example, Sun et al. put forward that electropulsing can instantly promote interface pre-melting under the coupling effect of the thermal effect and athermal effect of the electropulsing [34,35], and then affect the microstructure and performance of the metals and alloys [33,36]. Moreover, once the interface pre-melting occurs instantly under the effect of electropulsing, the occurrence of instant phase transition of 7075 aluminum alloy (with the surface temperature of the alloy sample increasing less than 303 K during EST) [32] and TC11 titanium alloy (with the surface temperature of the alloy sample rising less than 500 K during EST) [33] can also be reasonably explained. Thus, it was put forward that, if deftly coupling the Joule heat effect of the electropulsing and the electromagnetic oscillation effect of the EMP energy introduced by electropulsing, electromagnetic shocking treatment (EST) might, in a targeted manner, excite interface pre-melting of solid alloys with a relatively low surface temperature increase in the alloy sample. This probably attributes to the fact that the pre-melting (or melting) of the solid alloys is essentially a surface- or interface-initiated process activated by a continuous vibrational lattice instability or lattice shear instability [37,38], and this process would probably be activated by EMP during the EST [34,39]. When the interface pre-melting occurs, "local temporary directional mobility" at the interface region can be

achieved easily and then promote crack/void self-healing [1]. It indicates that healing induced by quasi-liquid might contribute to the metallic interface bridging or healing during the EST [32,33,35,36], and also to the crack/void healing of the metals and alloys by the electropulsing [8–12]. To further validate this analysis, in this work, an approximate in-situ experiment is specifically designed and then carried out by combining the sealing welding treatment (SWT) and the EST for TC11 alloys to explore the effect of EST on the self-healing of the metallic interface (or crack/void).

2. Materials and Methods

2.1. Raw Materials

Hot-forged TC11 alloy bars with typical (α + β) duplex microstructure used were provided by Northwest Institute for Non-Ferrous Metal Research (Xi'an, China). Their chemical composition was tested as Ti-6.5Al-3.2Mo-1.5Zr-0.3Si (wt.%). Firstly, rectangular specimens with dimensions of 5 mm × 10 mm × 55 mm were prepared [33,40]. Then, surfaces of the rectangular specimens, of dimensions of 10 mm × 55 mm, were chosen as the sealing surfaces to be prepared by simply mechanical grinding.

2.2. Sealing Welding Treatment

After that, sealing welding treatment (SWT) was carried out by Tungsten Inert Gas (TIG) welding, and the physical appearance of SWT samples is shown in Figure 1a. The soldering depth was checked as not more than 1.5 mm. Thus, for the SWT samples, an artificial interface of dimensions of about 7 mm × 52 mm was prepared.

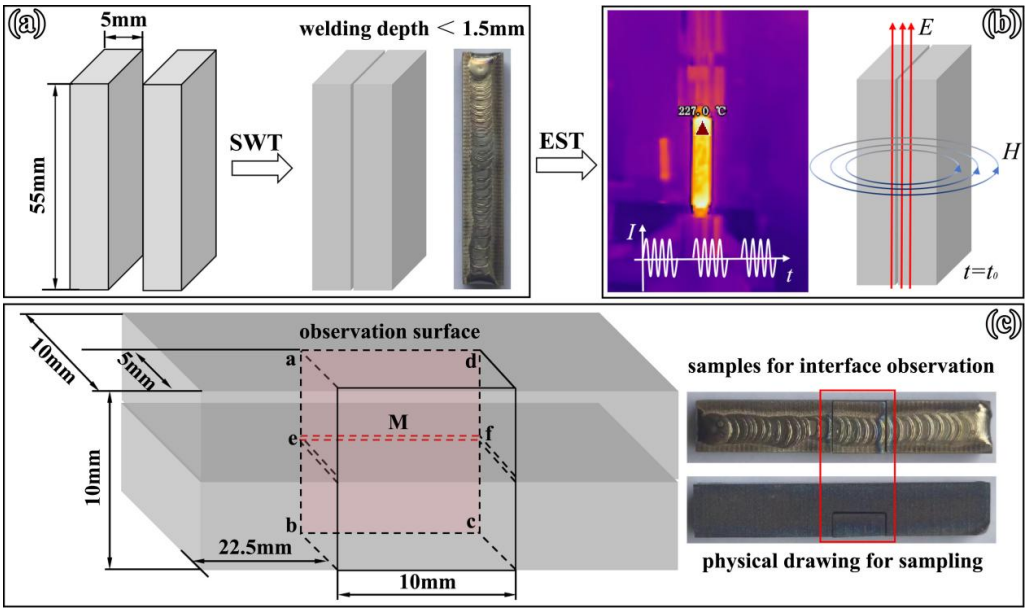

Figure 1. Schematic for SWT process and the physical appearance of SWT sample (**a**), the EST process (**b**), sampling process and physical drawing for sampling (**c**).

2.3. Electromagnetic Shocking Treatment

Then, one group of SWT samples were processed by the EST. The frequency of the used sinusoidal pulse current is 50 Hz. The actual electropulsing action time is 0.24 s (three discontinuous pulse trains and four pulses in per train) with a duty ratio of 16.7%; the pulse form is shown in Figure 1b. The peak current density is estimated as about 61.5 A·mm^{-2}. An infrared thermal camera was used to observe the temperature variation in the sample surface during the EST in real time. The highest temperature on the observed

sample surface (about 500 K) is near the electrode region because of the contact resistance (see Figure 1b). The temperature in the middle part of the sample is lower (less than 373 K).

2.4. SEM Observation

Finally, the sampling method of the interface M (or e–f region on a–b–c–d plane) for the observation is shown in Figure 1c. To exclude the influence of SWT on the interface to be observed, cubic samples with a dimension of 10 mm × 5 mm × 10 mm were cut from the middle of the samples, or a cutting depth of 5 mm was fixed. The SEM (Hitachi, S4800, Tokyo, Japan) was utilized to observe the interface morphology, to analyze the element distribution and phase distribution near the interface. Samples with the observation surface M were prepared by etching with a reagent (1.5 vol% HF + 4.0 vol% HNO_3 + 94.5 vol% H_2O) after mechanical grinding and polishing.

3. Results

The interface morphology of the SWT and (SWT + EST) samples is shown in Figure 2. For the SWT sample, as shown in Figure 2a,b, just as expected, the artificially made interfaces are nearly flat and mutually parallel. The interface spacing is about 1.35~1.76 μm. Actually, the interface morphology for the whole SWT sample is similar, and no interface bridging or healing can be observed.

However, for the (SWT + EST) sample, on one side of the surface, obvious fluctuation or oscillation, just like waves, occurs, as present in Figure 2c,d, in which the maximum interface spacing is about 1.45 μm. For the wavy surface, the distance between the highest and lowest points is approximately 0.91 μm (see Figure 2d). That is to say, there exists an obvious interface bridging tendency at some local regions in the (SWT + EST) sample, just as was put forward in Refs. [32,33,36]. Furthermore, it can also be observed that there exists obvious interface healing in local regions of the (SWT + EST) sample, as shown in Figure 2e. The length along the interface, which has reached complete healing is nearly 120 μm. Besides that, the EDS results in the completely healed interface region (see Figure 2f) demonstrate that, compared to those in the region slightly further away from the interface (Line 2), the average element compositions at the interface region (Lines 1 and 3) change little. Elements Al and Mo at the interface region (Lines 1 and 3) are a little higher than those in the region slightly further away from the interface (Line 2).

Next, to analyze whether phase transition occurs at the self-healed interface region, along the direction perpendicular to the interface (yellow lines in Figure 3a,b), the contents of the α and β phases near the interface region in the SWT sample and near the healed interface region in the (SWT + EST) sample, were analyzed by using Image-Pro Plus (6.0) software with three SEM images, respectively. The phase fraction of β phases (φ_β) of the SWT sample and the (SWT + EST) sample at the interface location and at the locations away from the interface (along the direction of the yellow lines in Figure 3a,b, take three locations above and below the interface, respectively), are analyzed, and three pictures are taken at each location for statistics and the average value taken. Finally, for the SWT sample and the (SWT + EST) sample, the total average values of the β phase content ($\varphi_{\beta\text{-ave}}$) are taken from the seven average values of the β phase content from the corresponding seven locations, as shown in Figure 3f. D represents the distance of the seven testing locations from the interface region.

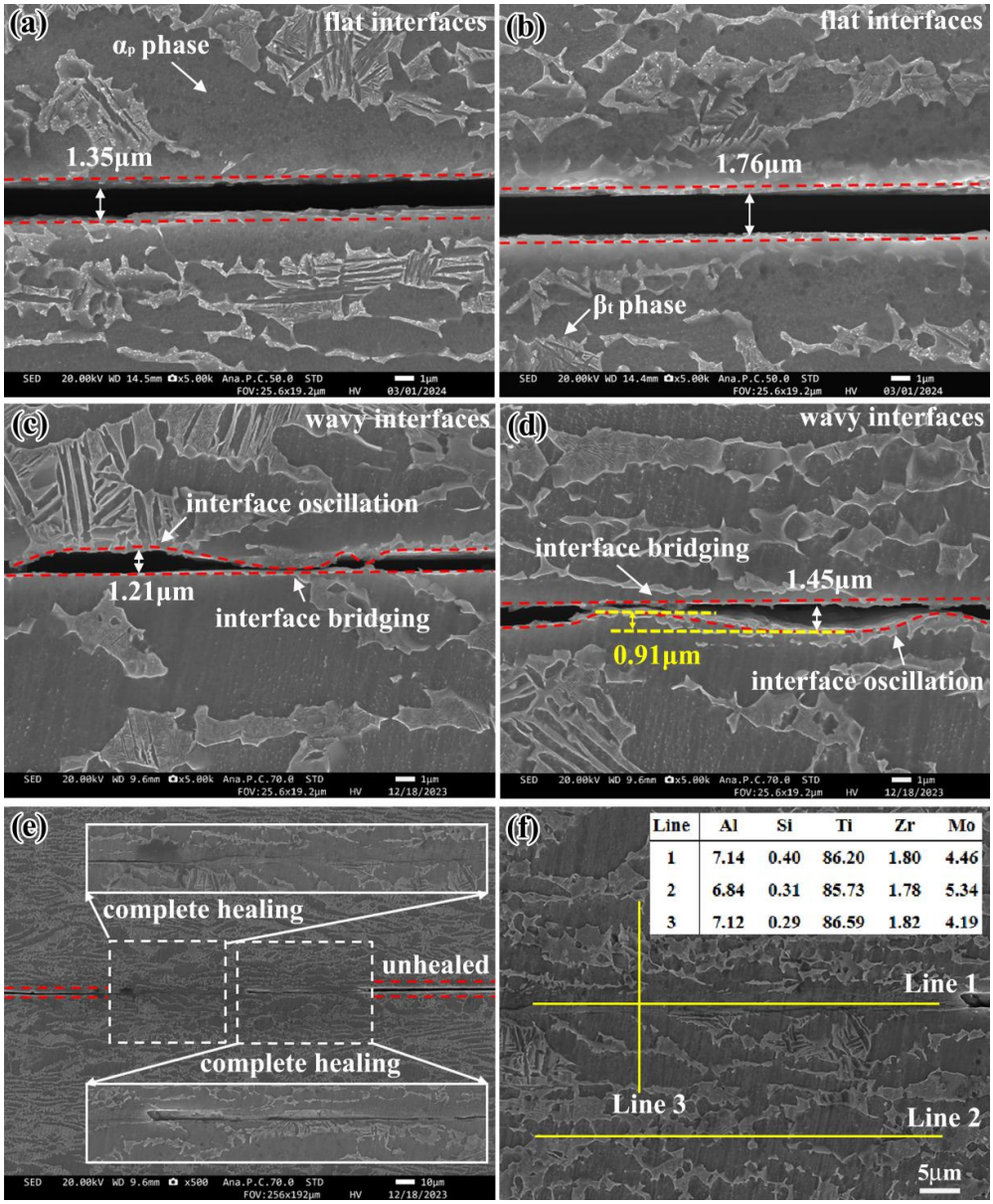

Line	Al	Si	Ti	Zr	Mo
1	7.14	0.40	86.20	1.80	4.46
2	6.84	0.31	85.73	1.78	5.34
3	7.12	0.29	86.59	1.82	4.19

Figure 2. SEM images of interface M for (**a**,**b**) SWT sample and (**c**–**f**) (SWT + EST) sample.

The corresponding statistical results presented in Figure 3f indicate that, compared to that of the SWT sample, the phase content distribution stays approximately unchanged for the (SWT + EST) sample. It indicates that, during the EST, in the case of promoting local interface healing of TC11 alloys, the action time of the electropulsing is short and the temperature rise caused by electropulsing is low; this is not enough to induce obvious phase content change in the interface region of the alloy sample. Simultaneously, observing the magnified SEM morphologies of the healed interface in the (SWT + EST) sample shown in Figure 3b, as presented in Figure 3c–e, the trace of healed interface is very visible; nevertheless, there still exists a trace of local areas that have not fully healed (indicated by arrows in Figure 3d).

According to Figures 2 and 3, it can be deduced that this kind of interface bridging and healing might be a result of surface migration. Moreover, whether observed from the micron scale or the nanoscale, this kind of interface bridging and healing distributes inhomogeneously or nonlinearly along the whole of the observed interfaces.

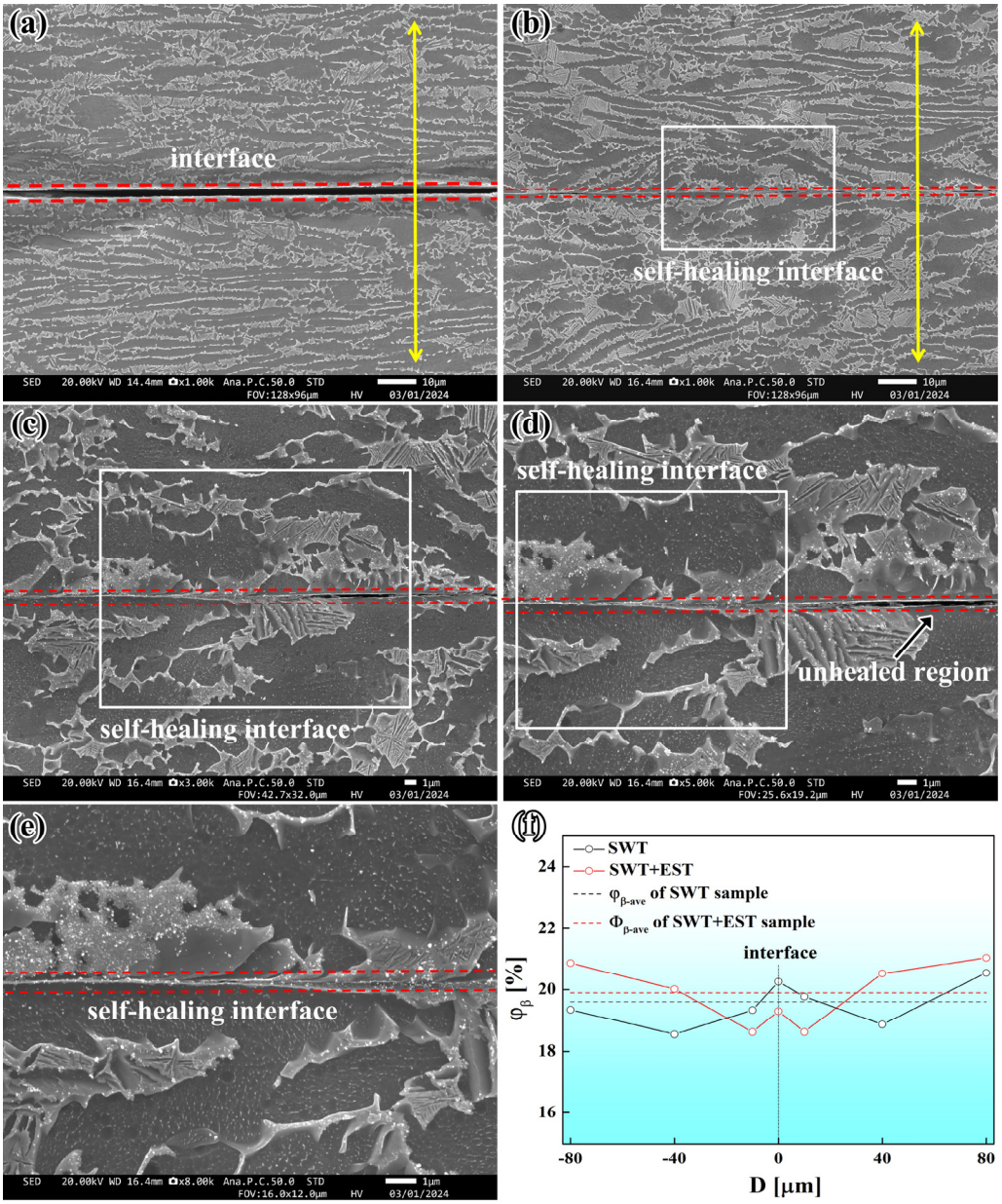

Figure 3. SEM morphology of interface M for the (**a**) SWT sample; (**b**–**e**) (SWT + EST) sample and the content distribution of β phase near interface region (**f**).

Furthermore, another observation surface was sampled to be investigated. Similarly, to exclude the influence of SWT on the interface complexion, cubic samples of dimensions of 10 mm × 4 mm × 10 mm were cut from the middle of the alloy samples and two symmetrical observation surfaces (N), with only ultrasonic cleaning, were obtained, as shown in Figure 4a. The results show that, just as expected, the surface morphology of the SWT sample is a typical mechanical grinding surface of solid alloys with visible scratches (see Figure 4b). However, for the (SWT + EST) sample, some of the surface morphology is also shown as a typical mechanical grinding surface, while the surface morphology in local regions X, shown in Figure 4c, looks very different. The gradually magnified surface morphology of this local region X is shown in Figure 4d–g. The distribution of the surface morphology in region X is of regularity, to some degree. On the one hand, "smooth areas" and "rough areas" exist in region X, and these two types of areas are arranged alternately, as shown in Figure 4e,f. On the other hand, the "rough areas" show a typical fracture surface morphology with typical micro cracks, fine "dimples" and tearing edges, while, at

some adjacent local areas, the surfaces are much smoother. It demonstrates that, for the (SWT + EST) sample, at these local "rough areas", interface bridging or healing probably occurred, while at the adjacent local "smooth areas", no interface bridging or healing occurred. This is consistent with the experimental results shown in Figures 2 and 3; that is, for the (SWT + EST) sample, interface bridging or healing occurred at local regions and this kind of bridging or healing arranges in an intermittent patterns or quasi-periodic arrangement.

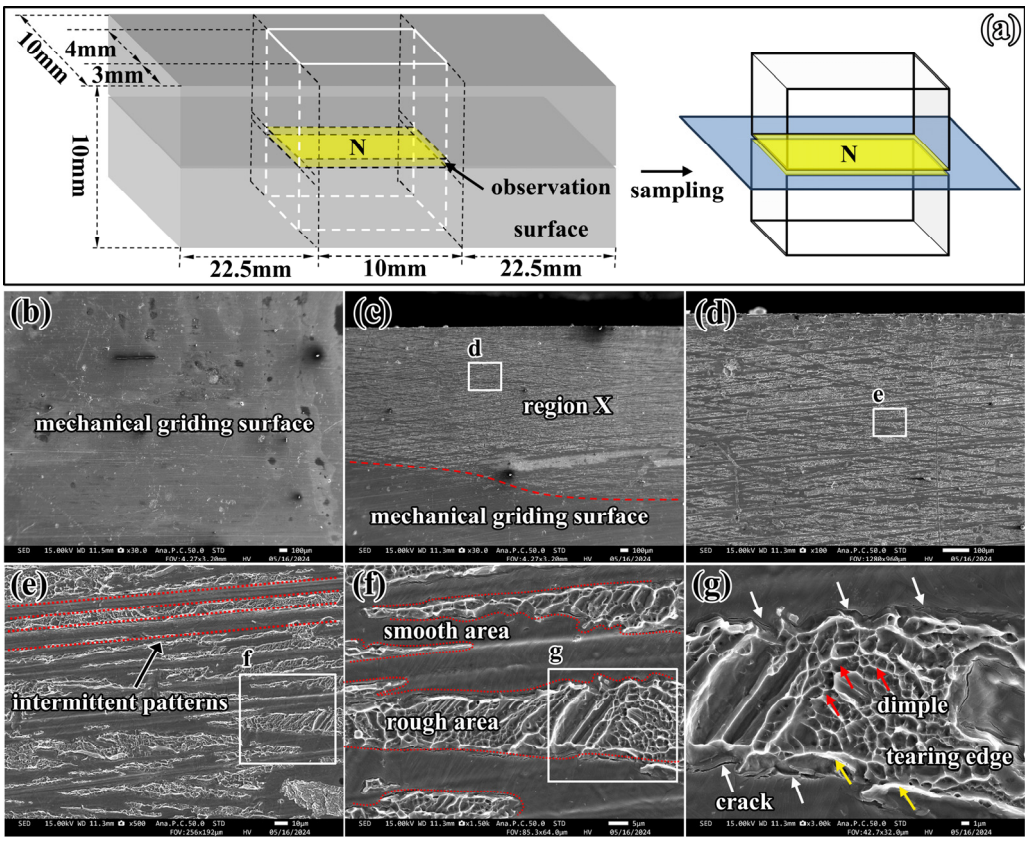

Figure 4. Sampling method of observation surface N (**a**); SEM morphology of surface N for the SWT sample (**b**) and (SWT + EST) sample (**c**–**g**).

4. Discussion

The above experimental results demonstrate that, under the condition that the element distribution and phase distribution at the interface area remain basically unchanged, EST promotes local interface bridging or self-healing of TC11 alloys with the sample surface temperature being limited to 500 K, which indicates that the local surface melting probably occurs during the EST. One possible reason is that the temperature at the local region of the sealed surface reaches the melting point of the bulk TC11 alloy sample. This is what most researchers can easily think of and generally support [8,11,14,15], which is also very difficult to directly verify by experiments or temperature simulation, as the local bridging and healing regions are distributed randomly and nonlinearly. Another possible reason is that this kind of pre-melting behavior probably does not attribute to just higher temperature but is due to the local vibration or shear instability of the superficial atoms under the coupling effect of electromagnetic oscillation and appropriate thermal activation [37–39]. Or, simply speaking, EST can promote alloy surface pre-melting locally, with relatively low temperatures, like how ice surface pre-melting can occur well below its bulk melting temperature (such as at 120 K [41]) as surface layers are more weakly bound

than those in the bulk [42]. No matter which one is closer to the truth, at the surface, local melting-like behavior, or pre-melting, indeed occurs.

Once the metallic surface tends toward pre-melting, it would have viscous characteristics, like fluid [43,44]. Then, the above experimental results can be clarified from another possible viewpoint. A second-order resonance system, including the mass system (superficial multiple atom layers), elastomer system (superficial ordered lattice) and viscoid system (superficial disordered atoms at the pre-melting zone), can be established, as shown in Figure 5a. In the presence of external force (such as EMP energy), the second-order resonance system satisfies the following equilibrium with the mathematical expression as [34],

$$\frac{d^2x(t)}{dt} + 2\xi\omega_n\frac{x(t)}{dt} + \omega_n^2 x(t) = \frac{F(t)}{m} \quad (1)$$

where $\xi = \eta/\left(2\sqrt{em}\right)$ is the damping ratio, with η being the viscosity coefficient of the viscoid, m being the mass of the system and e being the elasticity modulus of the elastomer, $\omega_n = \sqrt{e/m}$ is the intrinsic frequency of the system, $F(t)$ is the external input force and $x(t)$ is the output displacement of the system.

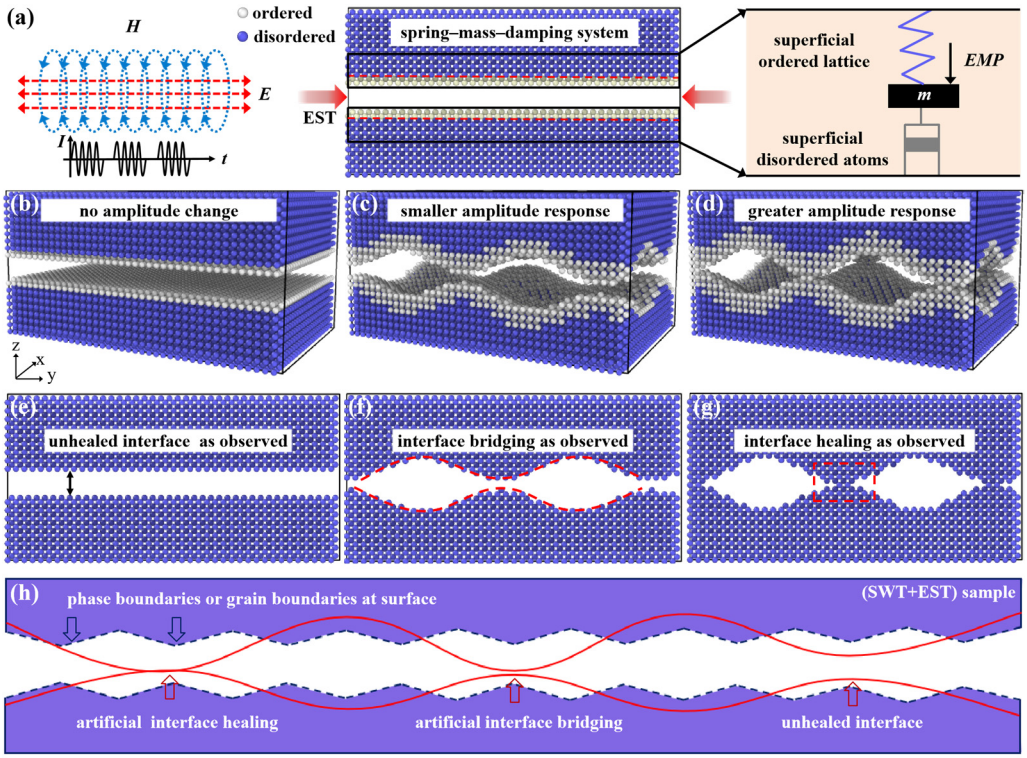

Figure 5. Modeling of the spring–mass–damping system for interface under EMP (**a**); Schematics for alloy interface evolution under EST (**b**–**h**).

As is widely known, when the angular frequency (ω) of the external input force is close to the intrinsic frequency of the system (ω_n), resonance will occur and the smaller the value of ξ, the more severe the vibration. Generally, the amplitude response function ($A(\omega)$) of the system can be expressed as,

$$A(\omega) = \frac{1}{\sqrt{\left((1-\Omega)^2\right)^2 + 4\xi^2\Omega^2}}, \Omega = \frac{\omega}{\omega_n} \quad (2)$$

Based on Equation (2), it can be analyzed that,

$$\begin{cases} \Omega = 0,\ A(\omega) = 1 \\ \Omega = 1,\ A(\omega) = \frac{1}{(2\xi)} \\ \Omega \to \infty,\ A(\omega) \to 0 \end{cases} \tag{3}$$

In this work, $\omega = 50$ Hz, $\Omega \neq 0$ and $\Omega \neq \infty$. Thus, based on Equation (3), when $\xi \geq 0.5$, the system amplitude is not larger than that of the input amplitude; only when $0 < \xi < 0.5$, is the system amplitude larger than that of the input amplitude. Then, the output displacement of the system with $\xi < 1$ can be expressed as,

$$x(t) = A_0 e^{-\xi\omega_n t}\sin(\omega t + \varphi) \tag{4}$$

where A_0 is a constant, φ is the phase angle. When $\xi \to 0$, $e^{-\xi\omega_n t} \to 1$.

Therefore, during the EST, under the coupling effect of appropriate thermal activation caused by electropulsing and electromagnetic oscillation caused by EMP, superficial atoms can be activated to oscillate as pulses with different amplitudes and different phases [45], turning increasingly disordered (white atoms) and having different viscosity characteristics. Then, according to Equation (3), under the excitation of discontinuous cEMP energy, atom layers at different positions on the surface respond with different amplitudes and phases. When these kind of oscillations end, these superficial atoms at different local positions probably stay with different output displacement ($x(t)$). According to Equation (3), if $\xi \geq 0.5$; no obvious amplitude change can occur for the system, as shown in Figure 5b,e, which is consistent with the unhealed interface region as observed in Figure 2e; while, if $\xi < 0.5$, the system amplitude is larger than that of the input amplitude and the interface complexion will probably change to an obvious extent. Thus, according to Equation (4), after the EST, one possible ideal scenario is that the displacement function for the superficial atoms (at surface 1 and 2) can be assumed as the following,

$$\begin{cases} F(x,y)_1 = 4\left[cos\left(x\cdot\frac{\pi}{30}\right) + cos\left(y\cdot\frac{\pi}{30}\right) + C_1\right] \\ F(x,y)_2 = 4\left[sin\left(x\cdot\frac{\pi}{30}\right) + sin\left(y\cdot\frac{\pi}{30}\right) + C_2\right] \end{cases} \tag{5}$$

where x and y represent different directions. Thus, the newly formed interface complexion for the alloy sample during the EST can be modeled as Figure 5c with a smaller amplitude response, and as Figure 5d with a greater amplitude response, forming some regular cellular structure. That is, during the EST, an increasing number of surface atoms absorb EMP energy and turn active or disordered. Then, some atoms move forward and others move backward along the direction perpendicular to the interface, which is another expression of the vibration instability (or shear instability if they have it) of superficial atoms, which can induce surface instability and then pre-melting [37]. The surface fluctuates like a (quasi-) pulse [46] (see Figure 2c,d) under the action of an excitation source (or electromagnetic oscillation), also indicating surface migration resulted from pre-melting, just as mentioned in some studies [42,43,47–49].

If similar oscillations occurred at two adjacent surfaces, interface bridging and even healing can easily occur locally and quickly, which would easily lead to some irreversible interface complexion evolution during the EST (see Figure 5c,d). The corresponding two-dimensional section view (cutting by y–z plane) of the alloy interface complexion is shown in Figure 5f,g. Actually, there are numerous phase boundaries (PBs) and grain boundaries (GBs) with different orientations (see blue dashed lines in Figure 5h) on the inside surface of the sealed (SWT + EST) sample. Considering that the occurrence of pre-melting is also affected by crystallographic face orientations, some crystallographic surfaces

are preferentially pre-melted [38,44] under the EST. Then, the oscillation of local PBs and GBs on surfaces during the EST can probably push the migration of macro surfaces like the way (red line) shown in Figure 5h, promoting the simultaneous occurrence of the unhealed interface, interface bridging and interface healing, which is basically consistent with the newly formed interface complexion for the (SWT + EST) sample observed in Figure 2.

5. Conclusions

(1) Without macro deformation and significant temperature increasing, EST can targetedly adjust interface complexion by interface pre-melting, such as promoting interface bridging and self-healing.
(2) Under the effect of EMP energy during the EST, coupling with appropriate thermal activation, alloy interface can energetically absorb EMP vibration energy and tends to occur nonlinear pre-melting.
(3) This work might provide new insights for the interface evolution mechanism of the solid alloys under the effect of EMP energy or (quasi-) periodic energy fluctuation as well as new design strategy of interface complexion modification of solid alloys by utilizing EMP energy or (quasi-) periodic energy fluctuation.
(4) Without significant surface temperature increasing and macro deformation, the EST can promote interface bridging and self-healing of the metals and alloys, which is benificial for the self-healing of micro cracks and the further improvement of the service performance of the metal parts.

Author Contributions: Conceptualization, Q.S.; Methodology, Y.D.; Validation, F.W. and W.J.; Formal analysis, S.L.; Investigation, Q.S. and Y.D.; Resources, S.L.; Data curation, F.W. and W.J.; Writing—original draft preparation, Q.S. and Y.D.; Writing—review and editing, Q.S.; Visualization, Y.D. and W.J.; Supervision, Q.S.; Funding acquisition, Q.S. All authors have read and agreed to the published version of the manuscript.

Funding: This work was financially supported by the National Natural Science Foundation of China (Grant No. 52273319), the 111 Project (Grant No. B17034) and Innovative Research Team Development Program of Ministry of Education of China (Grant No. IRT_17R83), the authors thank gratefully for their sincere appreciation.

Data Availability Statement: The original contributions presented in the study are included in the article. Further inquiries can be directed to the corresponding author.

Conflicts of Interest: The authors declare that they have no known competing financial interest or personal relationships that could have appeared to influence the work reported in this paper.

References

1. Dijk, N.V.; Zwaag, S.V.D. Self-Healing Phenomena in Metals. *Adv. Mater. Interfaces* **2018**, *5*, 1800226. [CrossRef]
2. Barr, C.M.; Duong, T.; Bufford, D.C.; Milne, Z.; Molkeri, A.; Heckman, N.M.; Adams, D.P.; Srivastava, A.; Hattar, K.; Demkowicz, M.J.; et al. Autonomous healing of fatigue cracks via cold welding. *Nature* **2023**, *620*, 552–556. [CrossRef]
3. Lu, Y.; Huang, J.Y.; Wang, C.; Sun, S.H.; Lou, J. Cold welding of ultrathin gold nanowires. *Nat. Nanotechnol.* **2010**, *5*, 218–224. [CrossRef]
4. Hu, X.G.; Guo, C.; Huang, Y.H.; Xu, Z.; Shi, Z.F.; Zhou, F.; Li, G.; Zhou, Y.; Li, Y.; Li, Z.Y.; et al. Liquid-induced healing of cracks in nickel-based superalloy fabricated by laser powder bed fusion. *Acta Mater.* **2024**, *267*, 119731. [CrossRef]
5. Zhang, J.Y.; Sun, M.Y.; Xu, B.; Hu, X.; Liu, S.; Xie, B.J.; Li, D.Z. Evolution of the interfacial microstructure during the plastic deformation bonding of copper. *Mater. Sci. Eng. A* **2019**, *746*, 1–10. [CrossRef]
6. Xie, B.J.; Yu, Z.X.; Jiang, H.Y.; Xu, B.; Wang, C.Y.; Zhang, J.Y.; Sun, M.Y.; Li, D.Z.; Li, Y.Y. Effects of surface roughness on interfacial dynamic recrystallization and mechanical properties of Ti-6Al-3Nb-2Zr-1Mo alloy joints produced by hot-compression bonding. *J. Mater. Sci. Technol.* **2022**, *96*, 199–211. [CrossRef]

7. Zhang, Z.; Ning, B.K.; Qian, W.F.; Wang, S.; Wang, N.; Chen, Y.N.; Li, Y.; Zhang, Q.Y.; Li, H.Z.; Wang, S.P.; et al. Promoting crack self-healing of nanocomposite coating by double slip systemic semi-coherent interface dislocation. *Mater. Res. Lett.* **2024**, *12*, 467–476. [CrossRef]
8. Song, H.; Wang, Z.J.; He, X.D.; Duan, J. Self-healing of damage inside metals triggered by electropulsing stimuli. *Sci. Rep.* **2017**, *7*, 7097. [CrossRef]
9. Zheng, X.G.; Shi, Y.N.; Lu, K. Electro-Healing cracks in nickel. *Mater. Sci. Eng. A* **2013**, *561*, 52–59. [CrossRef]
10. Lin, H.Q.; Zhao, Y.G.; Gao, Z.M.; Han, L.G. Effects of pulse current stimulation on the thermal fatigue crack propagation behavior of CHWD steel. *Mater. Sci. Eng. A* **2008**, *478*, 93–100. [CrossRef]
11. Hosoi, A.; Nagahama, T.; Ju, Y. Fatigue crack healing by a controlled high density electric current field. *Mater. Sci. Eng. A* **2012**, *533*, 38–42. [CrossRef]
12. Putz, B.; Glushko, O.; Cordill, M.J. Electromigration in Gold Films on Flexible Polyimide Substrates as a Self-healing Mechanism. *Mater. Res. Lett.* **2016**, *4*, 43–47. [CrossRef]
13. Zhou, L.Y.; Feng, S.B.; Sun, M.Y.; Xu, B.; Li, D.Z. Interfacial microstructure evolution and bonding mechanisms of 14YWT alloys produced by hot compression bonding. *J. Mater. Sci. Technol.* **2019**, *35*, 1671–1680. [CrossRef]
14. Wang, F.; Qian, D.S.; Hua, L.; Mao, H.J.; Xie, L.C. Voids healing and carbide refinement of cold rolled M50 bearing steel by electropulsing treatment. *Sci. Rep.* **2019**, *9*, 11315. [CrossRef]
15. Xie, L.H.; Guo, H.J.; Song, Y.L.; Hua, L.; Wang, L.Q.; Zhang, L.C. Novel approach of electroshock treatment for defect repair in near-β titanium alloy manufactured via directed energy deposition. *Metall. Mater. Trans. A* **2021**, *52*, 457–461. [CrossRef]
16. Cai, Z.P.; Qian, C.K.; Zhang, X.; Dai, N.; Wu, Y.; Ji, W. Mechanism and application of mechanical property improvements in engineering materials by pulsed magnetic treatment: A review. *Friction* **2024**, *12*, 2139–2166. [CrossRef]
17. Qian, C.K.; Liu, Q.; Xiong, X.Y.; Ye, B.J.; Li, Z.Y.; Li, K.J.; Ying, S.J.; Zhang, H.J.; Huang, D.M.; Zhang, X.; et al. Mechanism for magnetic field induced structural relaxation and accompanying fracture toughness improvement of the thermal spraying coating. *Mater. Des.* **2022**, *223*, 111113. [CrossRef]
18. Qian, C.K.; Liu, Q.; Li, K.J.; Ma, L.; Cai, Z.P. Electrochemical corrosion behavior variation of WC-10Co4Cr coating subjected to different magnetic treatments and its mechanism. *Corros. Sci.* **2024**, *229*, 111883. [CrossRef]
19. Li, Z.; Li, K.J.; Qian, C.K.; Wang, D.X.; Ji, W.; Wu, Y.; Cai, Z.P.; Liu, Q. Effect of pulsed magnetic field on retained austenite of quenched 8Cr4Mo4V steel under cryogenic condition. *J. Mater. Res. Technol.* **2023**, *23*, 5004–5015. [CrossRef]
20. Ye, Y.X.; Tang, C.; Zhang, Y.; Yang, Y.; Li, K.J.; Wang, F.; Huang, B.H.; Xu, L.J.; Gao, L.; Wang, J.H.; et al. Magnetic-assisted ultrasonic nanocrystal surface modification induced microstructures of titanium alloy. *Surf. Coat. Technol.* **2024**, *485*, 130892. [CrossRef]
21. Ao, D.; Zhang, H.; Wang, H.; Bao, W.; Gao, J.; Chu, X. Investigation of deformation behavior during electric pulse assisted incremental forming of Ti-6Al-4V sheet with a water-cooling system. *J. Manuf. Process.* **2024**, *126*, 165–174. [CrossRef]
22. Li, S.; Chen, L.; Chu, X.; Tang, J.; Zhao, G.; Zhang, C. Improvement in Mechanical Properties of Al-Zn-Mg Alloy by Applying Electric Pulse During Hot Extrusion. *J. Mater. Res. Technol.* **2020**, *9*, 1210–1220. [CrossRef]
23. Sun, F.; Wan, S.; Liao, J.; Wang, D.; Xiao, G.; Niu, Q. Effect of Electric Pulse Treatment on the Microstructure and Machining Performance of Ti-6Al-4V. *J. Mater. Eng. Perform.* **2024**, *33*, 1169–1178.
24. Kang, K.; Li, D.; Wang, A.; Shi, D.; Gao, G.; Xu, Z. Experimental Investigation on Aging Treatment of 7050 Alloy Assisted by Electric Pulse. *Results Phys.* **2020**, *16*, 103016. [CrossRef]
25. Ma, R.; Zhang, X. Refining the Microstructure to Strengthen Casting Titanium Alloy by Electric Pulse. *Mater. Sci. Eng. A* **2022**, *849*, 143519. [CrossRef]
26. Oboňa, J.V.; Ocelík, V.; Rao, J.C.; Skolski, J.Z.P.; Römer, G.R.B.E.; Huis, A.J.; De Hosson, J.T.M. Modification of Cu surface with picosecond laser pulses. *Appl. Surf. Sci.* **2014**, *303*, 118–124. [CrossRef]
27. Gu, S.; Liu, C.; Kimura, Y.; Yoon, S.; Cui, Y.; Yan, X.; Ju, Y.; Toku, Y. Realizing strength–ductility synergy in a lean duplex stainless steel through enhanced TRIP effect via pulsed electric current treatment. *Mater. Sci. Eng. A* **2023**, *883*, 145534. [CrossRef]
28. Zhang, X.; Zhang, J.; Yao, Y.; Qiao, Q.; Zhao, L.; Liu, L.; Jin, F.; Zhan, M.; Li, H. Anomalous enhancing effects of electric pulse treatment on strength and ductility of TC17 linear friction welding joints. *J. Mater. Sci. Technol.* **2024**, *203*, 155–166. [CrossRef]
29. Liu, D.; Liu, X.; Zhou, Y.; Zhang, Y.; Geng, G. Influence of electric pulse on microstructural characteristics and mechanical properties of cast AZ91D magnesium alloy. *J. Alloys Compd.* **2025**, *1010*, 177303. [CrossRef]
30. Ren, L.; Liu, C.H.; Zhang, X.F. Rapid repair of thermal aging embrittlement in 17-4PH martensitic stainless steel using pulsed electric current. *Mater. Charact.* **2024**, *208*, 113650. [CrossRef]
31. Xu, G.L.; Zhu, Y.Q.; Peng, L.J.; Mi, X.J.; Xie, H.F.; Cao, Y.C.; Li, X.H. Simultaneously enhancing the strength and ductility of Cu-Ti-Fe alloy through electric current pulse induced precipitation. *Scr. Mater.* **2025**, *255*, 116387. [CrossRef]
32. Sun, Q.; Liu, L.H.; Yu, S.; Wang, H.; Wang, H.J. Gradient phase transformation of Al-Zn-Mg-Cu alloy induced by nonlinear interface wetting under electromagnetic shocking treatment. *J. Mater. Sci.* **2023**, *58*, 16239–16255. [CrossRef]

33. Li, Y.F.; Wang, F.L.; Sun, Q.; Qian, D.S.; Song, Y.L.; Hua, L. Study on the microstructure and impact toughness of TC11 titanium alloy by a novel electromagnetic shocking treatment. *Mater. Sci. Eng. A* **2023**, *876*, 145149. [CrossRef]
34. Sun, Q.; Hua, L. Micro texture of titanium alloys excited nonlinearly by electromagnetic pulse. *Scr. Mater.* **2021**, *200*, 113828. [CrossRef]
35. Sun, Q.; Yu, Y.M.; Wang, F. A novel electromagnetic shock treatment to selectively modify grain boundary and improve the corrosion resistance of aluminium alloy. *Mater. Lett.* **2023**, *334*, 133703. [CrossRef]
36. Sun, Q.; Wang, H.J.; Yu, S.; Wang, F.; Song, Y.L.; Hua, L.; Qian, D.S. Reducing stress corrosion cracking susceptibility of high-strength aluminum alloy and its fastener by a novel electromagnetic shocking treatment. *J. Alloys Compd.* **2023**, *960*, 170917. [CrossRef]
37. Cahn, R.W. Materials science: Melting and the surface. *Nature* **1986**, *323*, 668–669. [CrossRef]
38. Tartaglino, U.; Zykova-Timan, T.; Ercolessi, F.; Tosatti, E. Melting and nonmelting of solid surfaces and nanosystems. *Phys. Rep.* **2005**, *411*, 291–321. [CrossRef]
39. Ding, K.; Oue, D.; Chan, C.T.; Pendry, J.B. Casimir-Induced Instabilities at Metallic Surfaces and Interfaces. *Phys. Rev. Lett.* **2021**, *126*, 046802. [CrossRef]
40. Jiang, W.B.; Kong, Q.P.; Cui, P. Further evidence of grain boundary internal friction in bicrystals. *Mater. Sci. Eng. A* **2010**, *527*, 6028–6032. [CrossRef]
41. Hong, J.N.; Tian, Y.; Liang, T.C.; Liu, X.M.; Song, Y.Z.; Guan, D.; Yan, Z.X.; Guo, J.D.; Tang, B.Z.; Cao, D.Y.; et al. Imaging surface structure and premelting of ice Ih with atomic resolution. *Nature* **2024**, *630*, 375–380. [CrossRef] [PubMed]
42. Slater, B.; Michaelides, A. Surface premelting of water ice. *Nat. Rev. Chem.* **2019**, *3*, 172–188. [CrossRef]
43. Kong, Q.P.; Fang, Q.F. Progress in the Investigations of Grain Boundary Relaxation. *Crit. Rev. Solid State Mater. Sci.* **2016**, *41*, 192–216. [CrossRef]
44. Danzig, A.; Scaly, O.; Polturak, E. Is the surface fluid during premelting? A study of the surface shear resistance of solid Gallium. *Surf. Sci.* **2021**, *705*, 121779. [CrossRef]
45. Li, X.; Zhu, Q.; Hong, Y.R.; Zhang, H.; Wang, J.; Wang, J.W.; Zhang, Z. Revealing the pulse-induced electroplasticity by decoupling electron wind force. *Nat. Commun.* **2022**, *13*, 6503. [CrossRef]
46. Bai, Z.T.; Misra, A.; Fan, Y. Universal Trend in the dynamic relaxations of tilted metastable grain boundaries during ultrafast thermal cycle. *Mater. Res. Lett.* **2022**, *10*, 343–351. [CrossRef]
47. Dillon, S.J.; Tang, M.; Carter, W.C.; Harmer, M.P. Complexion: A new concept for kinetic engineering in materials science. *Acta Mater.* **2007**, *55*, 6208–6218. [CrossRef]
48. Cantwell, P.R.; Tang, M.; Dillon, S.J.; Luo, J.; Rohrer, G.S.; Harmer, M.P. Grain boundary complexions. *Acta Mater.* **2014**, *62*, 1–48. [CrossRef]
49. Liss, K.D.; Xu, P.G.; Shiro, A.; Zhang, S.Y.; Yukutake, E.; Shobu, T.; Akita, K. Abnormal grain growth: A spontaneous activation of competing grain rotation. *Adv. Eng. Mater.* **2024**, *26*, 2300470. [CrossRef]

Disclaimer/Publisher's Note: The statements, opinions and data contained in all publications are solely those of the individual author(s) and contributor(s) and not of MDPI and/or the editor(s). MDPI and/or the editor(s) disclaim responsibility for any injury to people or property resulting from any ideas, methods, instructions or products referred to in the content.